SUPPLEMENTARY INFORMATION

Towards photoelectrochromic modulation of NIR absorption in plasmonic ITO using pentacene films

Anthony Maho[1,2,3], Dong Kuk Kim[1], Jessica Wade[1], Emma Bryan[1], Luc Henrard[4], Yoann Olivier[4], Stoichko D. Dimitrov[5], Rudi Cloots[2] and Sandrine Heutz[1,*]

[1] *Department of Materials and London Center for Nanotechnology, Imperial College London, London SW7 2BP, United Kingdom.*

[2] *Group of Research in Energy and Environment from Materials (GREENMAT), University of Liège, Quartier Agora – B6a, Sart-Tilman, 4000 Liège, Belgium.*

[3] *Univ. Bordeaux, CNRS, Bordeaux INP, ICMCB, UMR 5026, 87 Avenue du Docteur Schweitzer, 33600 Pessac, France.*

[4] *Department of Physics and Namur Institute of Structured Materials, University of Namur, Rue de Bruxelles 61, 5000 Namur, Belgium.*

[5] *Department of Chemistry, Queen Mary University of London, London E1 4NS, United Kingdom.*

[*] *Corresponding author: Prof. Sandrine Heutz, Department of Materials and London Center for Nanotechnology, Imperial College London, London SW7 2BP, United Kingdom. s.heutz@imperial.ac.uk*

1. TEM characterization of ITO nanocrystals

Figure S1 presents TEM images of plasmonic ITO nanocrystals (10% wt. Sn), (a) as obtained from colloidal synthesis and (b) following ligand-stripping reaction; a 6.0 ± 1.0 nm diameter value is determined (average value on 40 measurements).

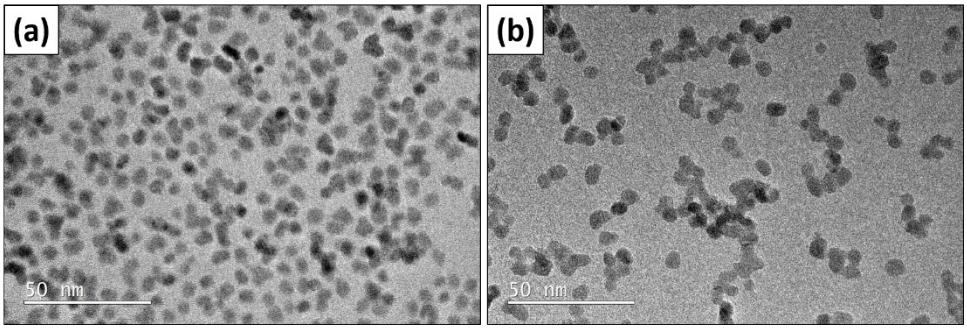

Figure S1. *TEM images of (a) as-synthesized ligand-capped and (b) ligand-stripped plasmonic ITO nanocrystals. Scale bars = 50 nm.*

2. Optical microscopy images of ITO, PEN and PEN-ITO layers

Figure S2 presents optical microscopy images and photographs of (a) ITO, (b) PEN and (c) PEN-ITO layers deposited on glass substrates.

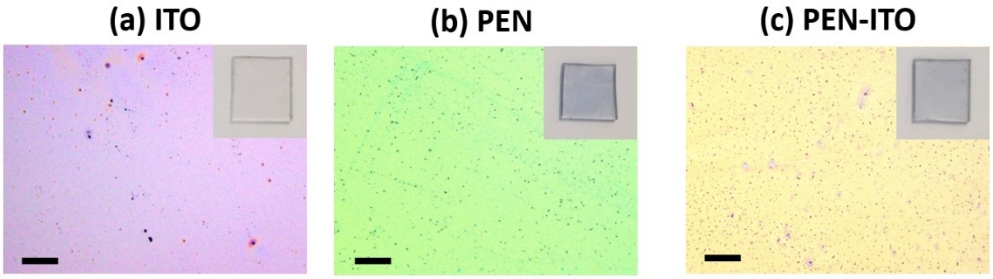

Figure S2. *Optical microscopy images of (a) ITO, (b) PEN and (c) PEN-ITO layers deposited on glass substrates. Scale bars = 100 µm. Insets: photographs of the corresponding samples.*

3. ATR-FTIR characterization of ITO, PEN and PEN-ITO layers

Figure S3 presents ATR-FTIR spectra of ITO, PEN and PEN-ITO layers deposited on glass substrates over (a) 1500-1250 cm^{-1} and (b) 920-840 cm^{-1} wavenumber ranges. Vibration bands characteristic of *X*, *Y* and *Z* modes by 1296, 1443 and 904 cm^{-1}, respectively, are highlighted with dashed vertical lines.[1,2]

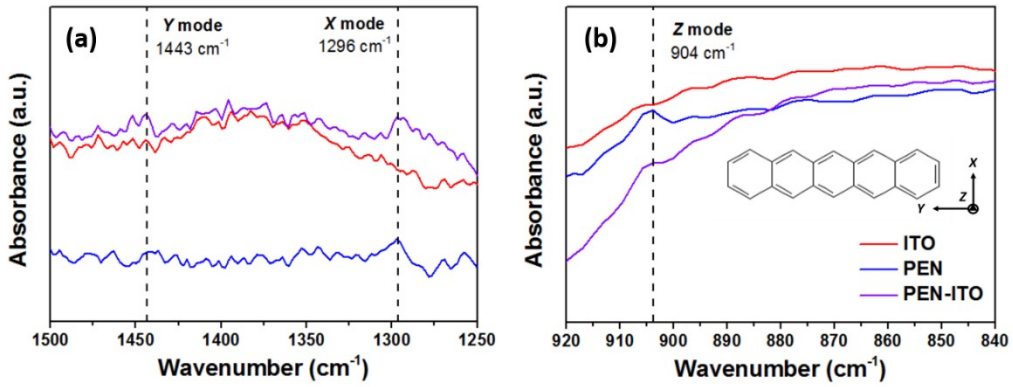

Figure S3. *ATR-FTIR absorbance spectra measured over (a) 1500-1250 cm^{-1} and (b) 920-840 cm^{-1} ranges of (a) ITO, (b) PEN and (c) PEN-ITO layers deposited on glass substrates. Inset: schematic view of pentacene's molecular structure.*

4. VIS-NIR characterization of ITO, PEN and PEN-ITO layers

Figure S4 presents optical data of ITO (red), PEN (blue) and PEN-ITO (purple) layers deposited on quartz substrates, obtained from VIS-NIR spectrometric measurements over a 400-2200 nm wavelength λ range.

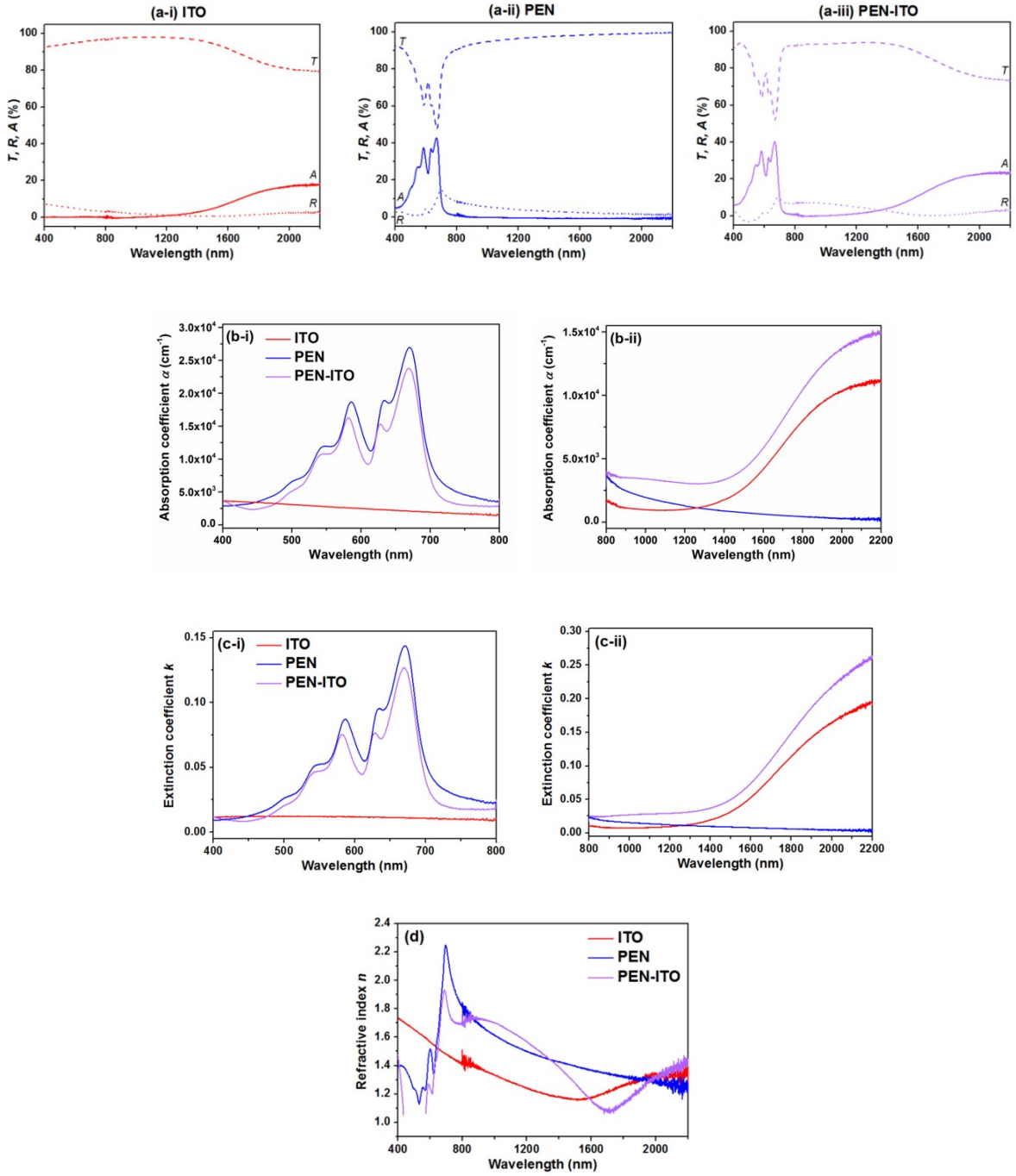

Figure S4. *VIS-NIR spectra of ITO (red curves), PEN (blue curves) and PEN-ITO layers (purple curves) deposited on quartz substrates: (a) evolution over wavelength* λ *of transmittance* T *(dashed lines), reflectance* R *(dotted lines) and absorptance* A *(solid lines); (b) absorption coefficient* α*, (c) extinction coefficient* k *and (d) refractive index* n*.*

Figure S4a shows (i) ITO, (ii) PEN and (ii) PEN-ITO samples transmittance *T* (dashed lines) and reflectance *R* (dotted lines), with bare quartz as 100% of *T* and 0% of *R*, from which absorptance *A* (solid lines) is derived as $A(\%) = 1 - T(\%) - R(\%)$. Peaks observed in VIS range (by λ < 800 nm) are correlated to pentacene electronic transitions, while decrease of *T* and increase of *R* in NIR range (by λ > 1400 nm) are correlated to ITO plasmon frequency. Note also that PEN-ITO bilayers present globally lower *R* values than PEN single layers, which translates as an "anti-reflective" effect occurring from the presence of the ITO layer being intercalated between the quartz substrate and the pentacene coating.

Figure S4b shows the evolution in (i) VIS and (ii) NIR of absorption coefficient α values in cm^{-1}, obtained as $\alpha = Abs/t$ with *Abs* being the measured absorbance (as $Abs = -\log T$) and *t* the layers thickness. A corrected *t* value is specifically implemented for the calculations related to the PEN-ITO sample, using 120 nm for the 400-800 nm range corresponding to the VIS-active PEN component, and 90 nm for the 800-2200 nm corresponding to NIR-active ITO component. Values of ~2.0-2.5 x 10^{-4} cm^{-1} measured in VIS for PEN and PEN-ITO samples, and of ~1.0-1.5 x 10^{-4} cm^{-1} in NIR for ITO and PEN-ITO samples, respectively, match those reported in literature.[3-5]

Figure S4c shows the evolution in (i) VIS and (ii) NIR of extinction coefficient *k*, obtained as $k = \alpha\lambda/4\pi$. Interestingly, *k* values in VIS are observed to decrease for pentacene molecules deposited on plasmonic ITO (purple curves, *vs*. blue curves for neat pentacene layers). This may be indicative of a lower degree of the *in-plane* component of their transition dipoles, and interpreted in the sense of a less perpendicular orientation with respect to the substrate surface – further confirming XRD, Raman and FTIR results presented and discussed above.[6,7]

Figure S4d shows the evolution of refractive index *n*, obtained as $n = \left(\frac{1+R}{1-R}\right) + \left(\frac{4R}{(1-R^2)} - k^2\right)^{1/2}$.[8,9] In agreement with literature, pentacene films present *n* values of ~1.1-1.5 by λ < 700 nm, which stands below bare quartz ones (typically of ~1.55); this can be interpreted as an anomalous dispersion behavior being due to a resonance effect between incident electromagnetic radiation and electrons polarization, leading to the coupling of the electrons to the oscillating electric field.[10] PEN-ITO bilayers show globally lower *n* values, being even inferior to 1 by the 435-575 nm wavelength range (and consequently figured as a gap on the corresponding curve); this obviously owes to measured *R(%)* values being slightly negative – *i.e.*, PEN-ITO presenting lower *R* values than bare quartz ones (see **Figure S4a**). This can be explained by a PEN-ITO sample structure provoking high scattering of light as well as enhanced resonance effects in pentacene due to increased electrostatic interactions, specifically caused by molecules being closer to each other in that surface configuration.

5. Tauc plots of ITO, PEN and PEN-ITO layers

Figure S5 presents Tauc plots calculated for PEN, ITO and PEN-ITO samples, plotting variations of $(\alpha h\nu)^2$ (direct band gap) in eV^2cm^{-2} in function of incident light energy $h\nu$ in eV. Band gaps energy values are estimated from the *x*-axis intersection point of the linear fit of the region(s) showing a steep, linear increase of light absorption (see dashed lines).[11]

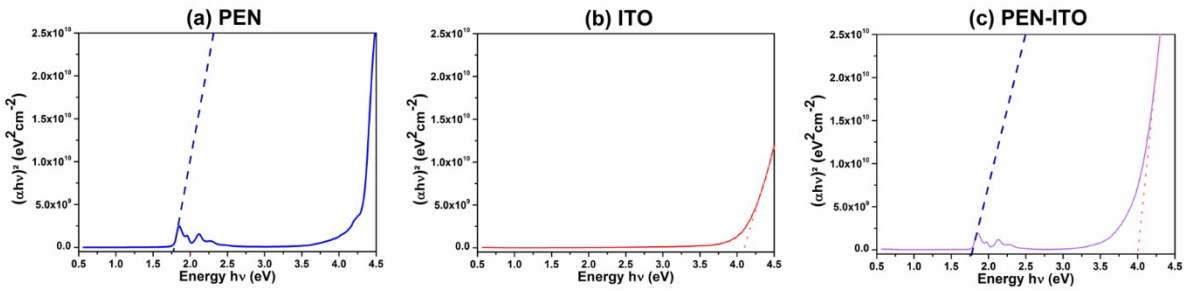

Figure S5. *Tauc plots of (a) pentacene (PEN) film deposited on quartz (blue curve), (b) plasmonic ITO layer deposited on quartz (red curve) and (c) PEN film deposited on ITO layer covered quartz (PEN-ITO, purple curve).*

6. Complementary TAS data

Figure S6 presents a global fitting analysis (by using the Optimus software) of the 840-1400 nm transient spectra of neat pentacene and ITO – pentacene, being performed to extract the time constant of the peak formation. **Figure S7** presents pentacene kinetic traces in VIS through samples probing at 665 nm (1.86 eV).

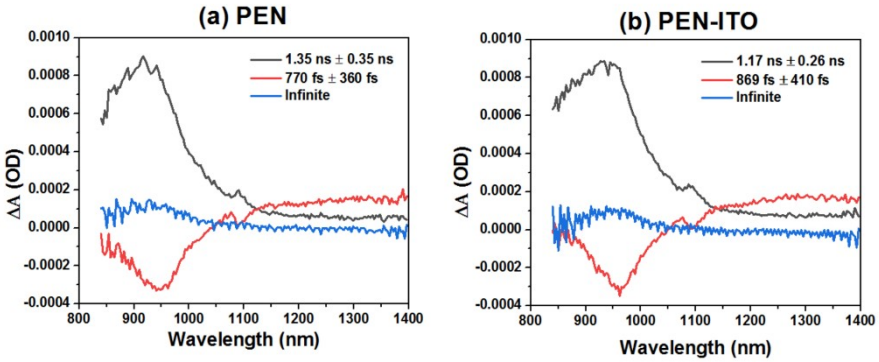

Figure S6. *Decay associated spectra of (a) PEN and (b) PEN-ITO received from global fitting analysis of the TA spectra from* ***Figure 5b-i*** *and* ***5b-ii****, respectively. The different time constants corresponding to each spectrum are defined with a different colour code.*

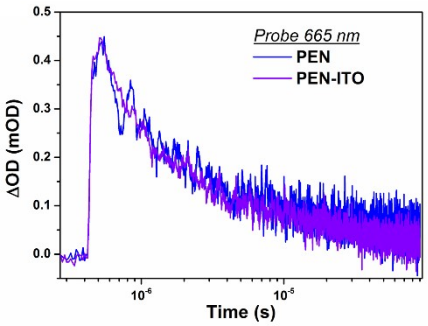

Figure S7. *Transient absorption dynamics of PEN film (blue curve) and PEN film deposited on ITO layer (PEN-ITO, purple curve) deposited on quartz substrates and measured at a probe wavelength of 665 nm corresponding to PEN absorption in VIS.*

7. Drude modeling of ITO nanoparticles and effective medium approach: effect of ω_p and ε_m

The dielectric function of ITO has been obtained by fitting the absorption of ITO nanoparticles dispersed in tetrachloroethylene (ε_m=2.5) with the extended Drude model proposed by Mergel *et al.* to model ITO,[12] *i.e.*:

$$\varepsilon_{ITO} = \varepsilon_\infty - \frac{{\omega_p}^2}{\omega^2 + i\omega\gamma} \quad \text{(S1)}$$

And:

$$\gamma = \gamma_L - \frac{\gamma_L - \gamma_H}{\pi}\left[arctan\left(\frac{\omega - \omega_x}{\omega_w}\right) + \frac{\pi}{2}\right] \quad \text{(S2)}$$

The following parameters are then obtained: ω_p= 1.97 eV, γ_L= 0.70 eV, γ_H= 0.00 eV, ω_x= 0.71 eV, ω_w= 0.17 eV, and ε_∞= 3.31.

The absorption cross section of an isolated spherical nanoparticle C_{ITO} follows as:

$$C_{ITO} = \frac{2\pi}{\lambda} I(\alpha) = \frac{8\pi^2}{\lambda}(R_{ITO})^3 I\left(\frac{\varepsilon_{ITO} - \varepsilon_m}{\varepsilon_{ITO} + 2\varepsilon_m}\right) \quad \text{(S3)}$$

With α being the polarizability of the sphere.

Figure S8 below presents the corresponding experimental absorption and fitted absorption cross section spectra.

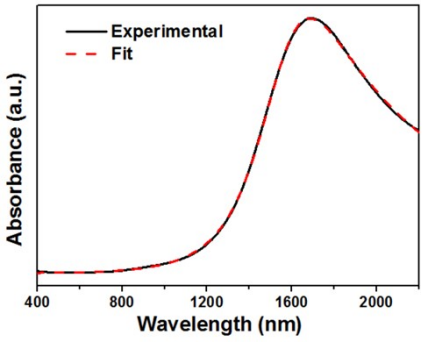

Figure S8. *Experimental absorption of ITO nanoparticles dispersed in tetrachloroethylene (solid black line), compared with absorption cross section of ITO nanospheres obtained from extended Drude modeling and the resulting fitted parameters (dashed red line).*

Then, to simulate the absorption of the ITO film, we consider the Maxwell-Garnett effective medium approach,[13] in which the medium dielectric function is given by:

$$\varepsilon_{film} = \varepsilon_m + \frac{3\eta_1\gamma_1}{1-\eta_1\gamma_1}\varepsilon_m \qquad \text{(S4)}$$

And:

$$\gamma_1 = \frac{\varepsilon_{ITO} - \varepsilon_m}{\varepsilon_{ITO} + 2\varepsilon_m} \qquad \text{(S5)}$$

The filling fraction $\eta_1$is set to 0.5. The absorption is then given by $\frac{2\pi}{\lambda} I(\varepsilon_{film})$.

Figure S9 below presents simulated absorption spectra of ITO nanoparticles and their corresponding evolution depending of ω_p and ε_m variations.

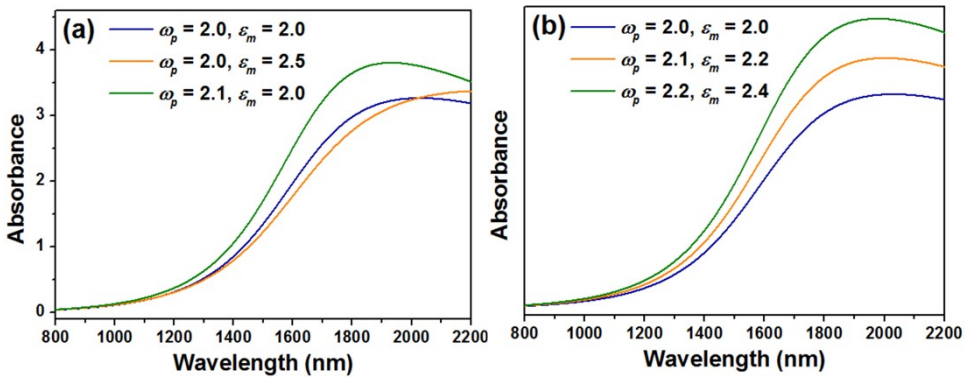

Figure S9. *Simulated (extended Drude modeling) absorption curves of ITO films constituted of nanoparticles of R = 3 nm: (a) impact of single change of ω_p or ε_m; (b) impact of combined change of ω_p and ε_m.*

REFERENCES FOR SUPPLEMENTARY INFORMATION

1 Y. Hosoi, K. Okamura, Y. Kimura, H. Ishii and M. Niwano, *Appl. Surf. Sci.*, 2005, **244**, 607.
2 E. Z. Fratczak, P. Uznanski and M. E. Moneta, *Chem. Phys.*, 2015, **456**, 49.
3 A. A. Serkov, H. V. Snelling, S. Heusing and T. Martins Amaral, *Sci. Rep.*, 2019, **9**, 1773.
4 C. Voz, J. Puigdollers, I. Martin, D. Munoz, A. Orpella, M. Vetter and R. Alcubilla, *Sol. Energy Mater. Sol. Cells,* 2005, **87**, 567.
5 B. Park, K. Whitham, K. Bian, Y.-F. Lim and T. Hanrath, *Phys. Chem. Chem. Phys.*, 2014, **16**, 25729.
6 A. Hinderhofer, U. Heinemeyer, A. Gerlach, S. Kowarik, R. M. J. Jacobs, Y. Sakamoto, T. Suzuki and F. Schreiber, *J. Chem. Phys.*, 2007, **127**, 194705.
7 E. Z. Fratczak, P. Uznanski and M. E. Moneta, *Chem. Phys.*, 2015, **456**, 49.
8 I. S. Yahia, Y. S. Rammah, S. AlFaify and F. Yakuphanoglu, *Superlattices Microstruct.*, 2013, **64**, 58.
9 G. F. Salem, E. A. A. El-Shazly, A. A. M. Farag and I. S. Yahia, *Optik*, 2018, **174**, 221.
10 I. S. Yahia, S. Alfaify, A. Jilani, M. S. Abdel-Wahab, A. A. Al-Ghamidu, M. M. Abutalib, A. Al-Bassam and A. M. El-Naggar, *Appl. Phys. B.*, 2016, **122**, 191.
11 P. Makula, M. Pacia and W. Macyk, *J. Phys. Chem. Lett.*, 2018, **9**, 6814.
12 D. Mergel and Z. Qiao, *J. Phys. D: Appl. Phys.*, 2002, **35**, 794.
13 T. C. Choy, *Effective Medium Theory*, Oxford University Press, Oxford, 2016.